催 化 学 报
2012 Chinese Journal of Catalysis Vol. 33 No. 7

文章编号: 0253-9837(2012)07-1125-08 国际版 DOI: 10.1016/S1872-2067(11)60399-9 研究论文: 1125~1132

$Au/CeO_2/SiO_2$ 催化 CO 低温氧化反应过程中 CeO_2 的作用

张慧丽, 任丽会, 陆安慧, 李文翠*

大连理工大学化工与环境生命学部化工学院精细化工国家重点实验室, 辽宁大连 116024

摘要: 采用具有分等级孔道结构的 SiO_2 (HMS) 为载体, 通过润湿浸渍引入少量 CeO_2, 经焙烧得到 CeO_2/HMS 复合载体, 然后采用沉积沉淀法负载上 Au 纳米粒子, 得到 Au/CeO_2/HMS 三元复合催化剂. 通过 X 射线衍射、程序升温还原和原位红外光谱等手段表征了催化剂的结构. 结果表明, CeO_2 的存在可控制 Au 颗粒的沉积并稳定载体上的纳米 Au 颗粒. Au/CeO_2/HMS 上 CO 低温氧化反应完全转化温度为 60 °C. 高度分散的 Au^0 可以活化 CO, CeO_2 颗粒则可以提供反应需要的氧. 稳定性测试结果显示, 反应 48 h 催化剂活性维持不变.

关键词: 二氧化硅; 一氧化碳氧化; 金; 二氧化铈; 稳定性

中图分类号: O643 **文献标识码**: A

收稿日期: 2012-02-14. 接受日期: 2012-03-26.

*通讯联系人. 电话/传真: (0411)84986140; 电子信箱: wencuili@dlut.edu.cn

基金来源: 国家自然科学基金 (20973031); 教育部新世纪优秀人才支持计划 (NCET-08-0075); 国家教育部博士点基金 (20100041110017).

本文的英文电子版(国际版)由Elsevier出版社在ScienceDirect上出版(http://www.sciencedirect.com/science/journal/18722067).

Role of CeO_2 in Three-Component $Au/CeO_2/SiO_2$ Composite Catalyst for Low-Temperature CO Oxidation

ZHANG Huili, REN Lihui, LU Anhui, LI Wencui*

State Key Laboratory of Fine Chemicals, School of Chemical Engineering, Faculty of Chemical, Environmental and Biological Science and Technology, Dalian University of Technology, Dalian 116024, Liaoning, China

Abstract: Hierarchical composite nanostructure composed of Au, CeO_2, and SiO_2 was fabricated by sequentially depositing ceria nanoparticles through impregnation and calcination, and then gold nanoparticles through a deposition-precipitation method on hierarchical monolithic silica (HMS) with multi-length scale pore structure. The Au/CeO_2/HMS composite nanostructure was characterized by X-ray diffraction, temperature-programmed reduction, and diffuse reflectance infrared Fourier transform spectroscopy. The results indicate that the presence of ceria had a significant effect on targeted deposition and stabilization of small metallic gold nanoparticles on the support. The temperature for complete conversion of CO to CO_2 over Au/CeO_2/HMS is ca. 60 °C at a space velocity of 80000 ml/(g·h). The highly dispersed metallic gold nanoparticles can activate CO and the small ceria nanoparticles supply oxygen in the reaction. The catalytic activity remains considerably stable during 48 h stability testing. The interaction between gold and ceria contributed greatly to CO oxidation and the presence of silica improved the stability of the gold catalyst.

Key words: silica; carbon monoxide oxidation; gold; ceria; stability

Received 14 February 2012. Accepted 26 March 2012.

**Corresponding author. Tel/Fax: +86-411-84986140; E-mail: wencuili@dlut.edu.cn*

This work was supported by the National Natural Science Foundation of China (20973031), the Program for New Century Excellent Talents in University of China (NCET-08-0075), and the Ph.D. Programs Foundation of Ministry of Education of China (20100041110017).

English edition available online at Elsevier ScienceDirect (http://www.sciencedirect.com/science/journal/18722067).

In the past years gold nanocatalysis has been extensively studied for low temperature CO oxidation [1–4], selective oxidation [5], selective hydrogenation [6], water-gas shift reaction [7], and decomposition of NO_x [8]. Besides the size

of the gold particles and the preparation methods, the nature of the support is also considered to be a key factor affecting the catalytic activity and stability of supported gold catalysts. Though transition metal oxide supported gold shows very high activity in many reactions, such kind of catalyst is considered to be susceptible to deactivation [9–11]. For example, the deactivation of Au/CeO_2 catalysts is primarily attributed to the blockage of active sites by carbonates and/or formates, the formation of which is facilitated by oxygen deficient sites on ceria surfaces [12].

Silica materials are commonly used as catalyst support with many excellent properties such as high thermal stability and high surface area (higher than those of reducible oxides) [13,14]. However, due to the low value of the point of zero charge (PZC) of SiO_2 (close to 2), the surface of silica is charged negatively at a pH higher than that value [15]. At the higher pH needed to precipitate $Au(OH)_3$ the highly negatively charged surface of SiO_2 does not allow the adsorption of $[Au(OH)_nCl_{4-n}]^-$ species onto the support surface, which is necessary for the formation and stabilization of small gold particles [16]. Au/mesoporous SiO_2 samples have been synthesized via several alternative routes to overcome this barrier: (1) modification of mesoporous SiO_2 by organic functional groups followed by loading gold [17]; (2) using $Au(en)_2Cl_3$ as the precursor [18]; (3) loading gold nanoparticles by vapor deposition on the surface of silica instead of using wet-chemistry methods [19,20]; (4) mixing Au^{3+} [21–25] or gold colloids [26–29] with SiO_2 source to facilitate the incorporation of gold nanoparticles in a silica matrix; (5) using ammonia as the precipitating agent so that the formed gold species was an ammino-hydroxo or an ammino-hydroxo-aquo gold cation complex $[Au(NH_3)_2(H_2O)_{2-x}(OH)_x]^{(3-x)+}$ [30]. In addition, a non-reducible and inherently ‘‘inert’’ SiO_2 support does not supply reactive oxygen for CO oxidation. In contrast, CoO_x, Fe_2O_3, ZnO, NaOH, CeO_2, and similar supports are reducible, inherently ‘‘active’’ and are thought to activate and store oxygen [31–35].

Recently, Carrettin et al. [36] reported that Au deposited on nanocrystalline particles of CeO_2 showed an increase of two orders of magnitude in the catalytic activity relative to the Au/CeO_2 catalysts prepared by Au deposition on a regular CeO_2 support. However, Moreau et al. [37] have demonstrated that the gold particles supported on pure metal oxides (e.g. CeO_2) are less stable than those supported on mixed oxide supports. Hence, Qian et al. [38] prepared CeO_2/SiO_2 supports by different methods and pretreated these supports at varying temperatures. After Au loading, the $Au/CeO_2/SiO_2$ catalysts showed a good stability; however, CO conversion reached only 10% at about 60 °C.

In the present study, we chose hierarchical monolithic silica (HMS) as matrix to combine with a small amount of ceria for supporting gold nanoparticles. Noticeably, HMS has unique properties (i.e. multi-length scale pore structures with fully developed and interconnected macropores and mesopores) [39], which are beneficial for mass transfer. In this way a highly active three-component $Au/CeO_2/HMS$ composite catalyst for CO oxidation was prepared. Detailed characterization gave insight into the adsorpotion sites of CO and the role of ceria in the composite catalyst.

1 Experimental

1.1 Preparation of hierarchical composite nanostructure

The HMS was prepared according to the established procedure [39,40]. Briefly, tetraethoxysilane (TEOS) and polyethylene glycol (PEG) ($M_w \approx 35000$) were dissolved in aqueous nitric acid. The molar ratio of the starting composition was $TEOS:HNO_3:H_2O:PEG = 1.00:0.25:14.69:7.77 \times 10^{-4}$. The sol was aged at 40 °C for 3 d to form the gelled monolith. The monolith was treated for 9 h in a 1.0 mol/L NH_4OH solution at 90 °C, and then neutralized with 0.1 mol/L HNO_3 and washed with acetone. The product HMS was collected after a drying at 40 °C and then calcined at 550 °C under air.

An aqueous solution of $Ce(NO_3)_2{\cdot}6H_2O$ was used as the ceria precursor and impregnated into this monolithic silica HMS. The sample was dried at 50 °C for 4 h and then calcined at 300 °C for 2 h in a muffle oven under air to obtain CeO_2/HMS composites. Gold nanoparticles were deposited on the as-synthesized CeO_2/HMS composites using a deposition-precipitation (DP) method with urea as the precipitating agent. Typically, 0.3 g composite support was added to 25 ml aqueous solution of $HAuCl_4$ and urea (molar ratio of urea:Au = 100:1). The suspension was then heated to 80 °C under vigorous stirring for 6 h. Finally the obtained product was filtered and washed with pure water. The resulting powder was dried at room temperature overnight in a vacuum desiccator. The obtained catalyst was denoted as $Au/CeO_2/HMS$. Approximately 3 wt% of gold and 10 wt% of ceria were deposited on the silica support. For comparison, silica alone was also used as support for gold nanoparticles loaded using the DP method as described above. The obtained catalyst was denoted as Au/HMS.

1.2 Characterization

Powder X-ray diffraction (XRD) was performed on a Philips X’pert PRO X-ray diffractometer (Cu K_α radiation, λ = 0.154178 nm). N_2 adsorption was performed at –196 °C using a Micromeritics Tristar 3000 instrument following sample pre-treatment at 120 °C under vacuum for 4 h. The

surface area (A_{BET}) was calculated using the Brunauer-Emmett-Teller (BET) model. The spent catalyst was characterized with a Hitachi HF2000 high resolution transmission electron microscope (HR-TEM) equipped with a cold field emission emitter at a beam energy of 200 kV and a cooled Si(Li) energy-dispersive X-ray (EDX) spectrometer from ThermoNoran Instruments for point resolved elemental analysis. More than 18 points were tested in order to obtain statistically reliable data. The diffuse reflectance infrared Fourier transform spectroscopy (DRIFTS) experiments were carried out on a Bruker Vector 22 FTIR spectrometer equipped with an MCT detector and a Harrick diffuse reflectance accessory. In situ DRIFT measurements were performed under the same conditions as the catalytic activity measurements. Background signals from gas-phase CO were subtracted from the reported spectra. Temperature programmed reduction (H_2-TPR) experiments were performed on a home-made device using a 8% H_2-92% N_2 mixture (30 ml/min flow) at a heating rate of 10 °C/min. Sieved catalyst (40 mg, 250–500 μm) was used. The sample was pretreated at 150 °C for 2 h and then cooled to room temperature in N_2 at a rate of 30 ml/min. The consumption of H_2 during the TPR experiment was measured by a thermal conductivity detector (TCD). X-ray photoelectron spectroscopy (XPS) measurements were performed on an Axis Ultra instrument of Kratos. The binding energies (BE) were referenced to the C 1*s* peak (284.9 eV) to account for the charging effect. The gold content of the catalysts was analyzed by inductively coupled plasma atomic emission spectrometer (ICP-AES) on an Optima 2000DV instrument.

1.3 Catalytic activity measurement

The catalytic activities in CO oxidation were measured using 50 mg of sieved composite (250–500 μm) in a gas mixture (1% CO, 20% O_2, and N_2 remainder at a flow rate of 67 ml/min, corresponding to a space velocity of 80000 ml/(g·h)). The reactant and product composition were analyzed by a GC 7890T gas chromatograph equipped with a thermal conductivity detector. Before catalytic tests, the composites were pretreated in a mixture of nitrogen and hydrogen (6:1 volume ratio, flow rate of 40 ml/min) at 250 °C for 2 h.

2 Results and discussion

2.1 Nanostructure and catalytic performance of Au/CeO_2/HMS

The hierarchical structure of the HMS is characterized by SEM and nitrogen adsorption measurement. Figure 1 shows the SEM image of HMS. The fully interconnected, sponge-like macroporosity of the silica monolith can be clearly seen in Fig. 1.

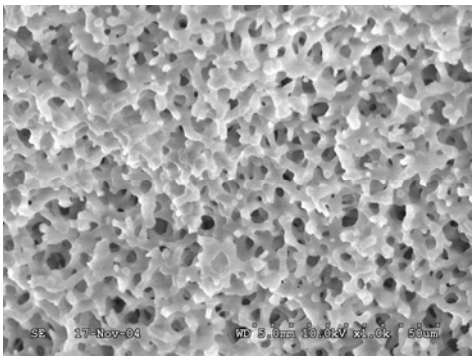

Fig. 1. SEM image of HMS.

The mesoporosity of the monolith was verified by measurement of nitrogen adsorption isotherm (Fig. 2). The nitrogen uptake at relative pressures above $p/p_0 = 0.9$ is due to filling of the textural pores. The pore size distribution is based on the Barrett-Joyner-Halenda (BJH) model and shows this silica monolith has the peak pore diameter around 24 nm in size. Combining the characterization results of SEM and nitrogen adsorption, the hierarchical structure (mesopores and macropores) of this HMS can be confirmed. The determined BET surface area of this HMS is 256 m^2/g. After introduction of ceria and gold nanoparticles, the surface area of Au/CeO_2/HMS is lowered to 179 m^2/g.

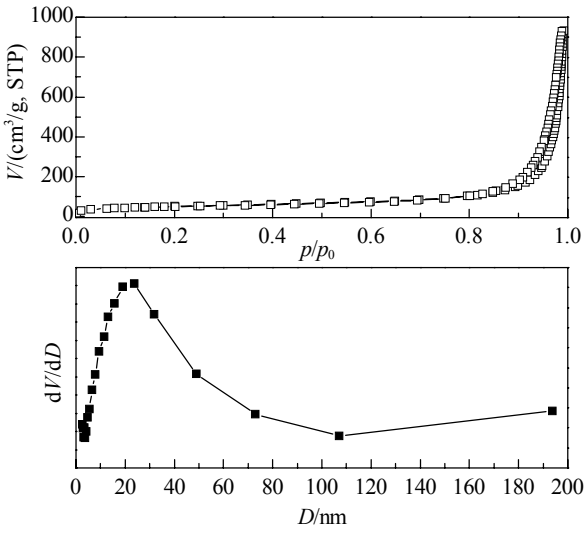

Fig. 2. N_2 adsorption isotherm and pore size distribution of HMS.

The prepared Au/CeO_2/HMS catalyst was characterized by XRD and the result is shown in Fig. 3. The peaks at 2θ = 28.6°, 33.1°, 47.5°, and 56.3° are ascribed to the (111), (200), (220), and (311) planes of ceria, respectively. The peaks at 2θ = 38.2° and 44.3° indicate the existence of metallic gold nanoparticles. The broad reflection peaks indicate that the particle sizes of both ceria and gold are small. The

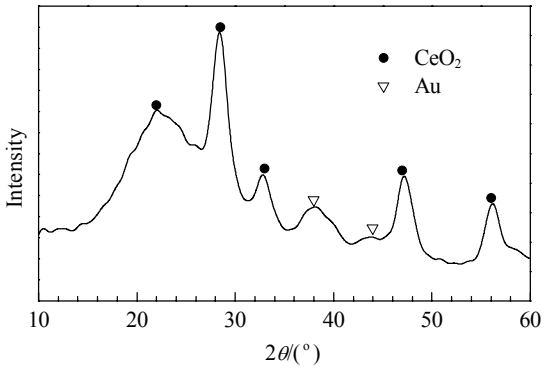

Fig. 3. XRD pattern of Au/CeO_2/HMS.

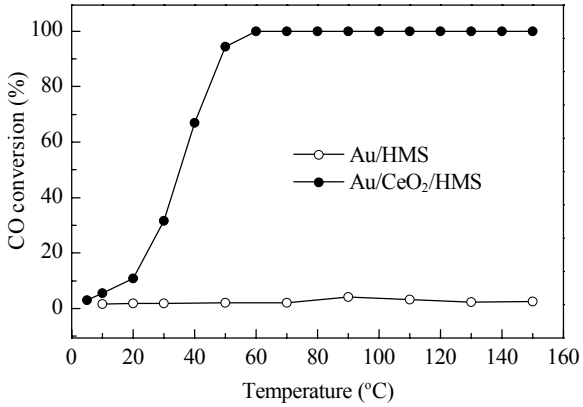

Fig. 4. Performance of Au/CeO_2/HMS and Au/HMS in the CO oxidation reaction. Reaction conditions: 50 mg of catalyst in a gas mixture (1% CO, 20% O_2, and N_2 balance) at a flow rate of 67 ml/min, corresponding to a space velocity of 80000 ml/(g·h).

estimated gold and ceria particle size (using the Scherrer equation) of the Au/CeO_2/HMS is ca. 2.5 and 5 nm, respectively.

The Au/CeO_2/HMS catalyst was tested in the CO oxidation reaction. For comparison the Au/HMS catalyst was also tested. The catalytic activities are displayed in Fig. 4. The results show that no obvious CO conversion was observed for the Au/HMS catalyst in the temperature range of 10 to 150 °C. After introducing 10 wt% ceria on the silica surface, Au/CeO_2/HMS exhibited a high activity with a complete conversion of CO to CO_2 ($T_{100\%}$) at ca. 60 °C, demonstrating the promoting effect of ceria. The TOF of the Au/CeO_2/HMS was calculated as about 0.32×10^{-3} h^{-1} at 20 °C, which lies between the values of Au/SiO_2 (0.26×10^{-3} at 20 °C) [41] and Au/CeO_2 catalysts (1.24×10^{-3} at 20 °C) [42].

The content of gold in the Au/HMS composite was determined as 4.05 wt% by the ICP-AES technique. However, large gold nanoparticles with 10–40 nm size were observed by TEM measurement after catalytic testing (Fig. 5(a)), which should be related to the poor catalytic activity for CO oxidation [43]. In contrast, in the TEM image of the Au/CeO_2/HMS composite (Fig. 5(b)), the gold and ceria nanoparticles are homogeneously dispersed on the silica support and largely located within the mesopores. Most particles are quite small and in the range of 2–5 nm even after the catalytic test, which is consistent with the value calculated from the XRD patterns. In order to verify whether the active components were homogeneously distributed over the entire samples, EDX analysis was performed and more than 18 points were randomly recorded by EDX from different parts of the sample. A representative result is shown in Fig. 5(c). It can be seen that the EDX results of the composite nanostructure also show the uniform and high dispersion degree of gold and ceria on the entire silica support. The sample Au/CeO_2/HMS possesses homogenous dispersion with average contents of 3.02 wt% gold and 9.80 wt% ceria. These are almost identical with the theoretical amounts according to the preparation.

In addition, the stability of the Au/CeO_2/HMS catalyst was evaluated to confirm whether both the gold and ceria active components could withstand long-time operation without an obvious loss of activity. Firstly, the sample was continuously run in the reactant mixture for 800 min at 60 °C (Fig. 6). During the catalytic run the conversion remained almost constant (100%) at the temperature of 60 °C. The composite was then stored in the reactor under nitrogen atmosphere overnight. Subsequently, the sample was tested

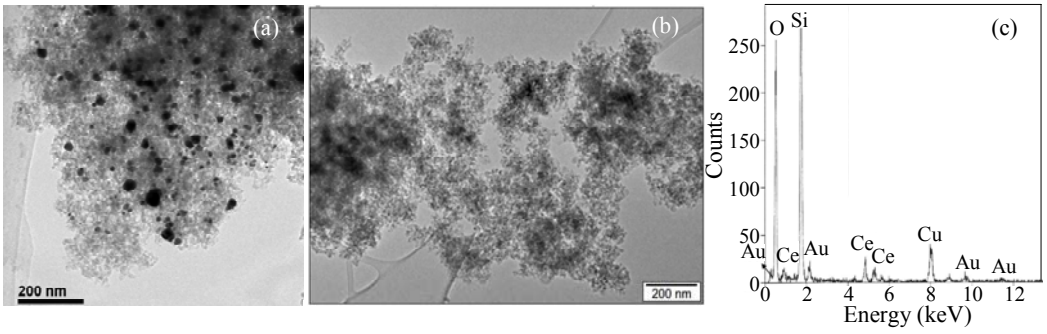

Fig. 5. TEM images of Au/HMS (a) and Au/CeO_2/HMS (b), and a representative EDX result of Au/CeO_2/HMS (c).

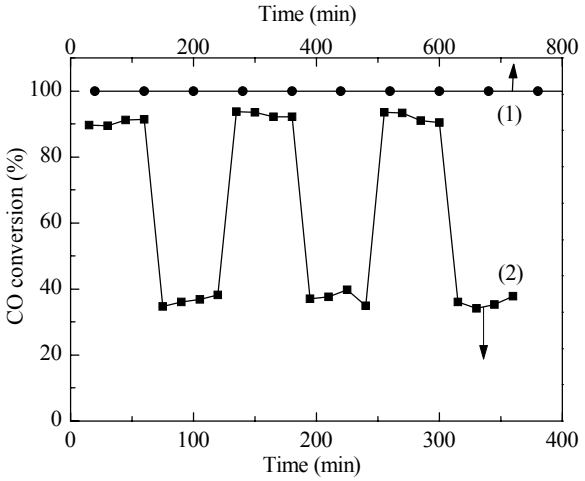

Fig. 6. Stability of Au/CeO_2/HMS composite. The stability test was performed first at 60 °C in a gas mixture (1% CO, 20% O_2, and N_2) at a space velocity of 80000 ml/(g·h) for 800 min (1), and then at 30 and 50 °C in sequence (2).

at temperatures of 30 and 50 °C, respectively. The resulting CO conversion only showed a slight decrease in catalytic activity. After 2 d testing at different conditions no obvious decrease in CO conversion confirmed that this catalyst is stable under the present reaction conditions.

2.2 Mechanistic insight into the action of the composite nanostructure

In order to precisely understand the role of ceria, HR-TEM, H_2-TPR, in-situ DRIFT, and XPS measurements were used to characterize the properties of the catalyst Au/CeO_2/HMS. HR-TEM measurements allow us to distinguish between the ceria and gold nanoparticles based on the lattice fringes. As can be seen in Fig. 7, the spacing of 0.32 nm is ascribed to the (111) planes of ceria, while 0.23 nm is assigned to the (111) planes of gold. The gold nanoparticles in Au/CeO_2/HMS are mostly deposited on or near the surface of the ceria, which gives a highly active CO oxidation catalyst [44].

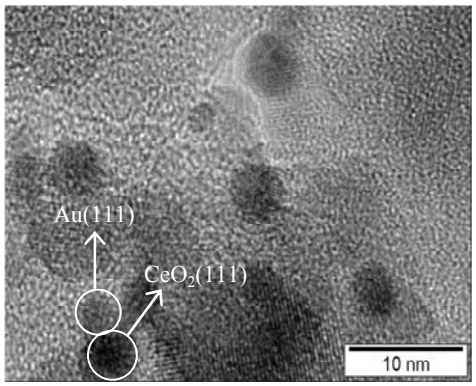

Fig. 7. HR-TEM image of Au/CeO_2/HMS after catalytic measurement.

The interaction between ceria and gold can also be verified by H_2-TPR profiles. As shown in Fig. 8, the peak at 180 °C in the Au/HMS trace should be due to the reduction of Au^{3+} to Au^+/Au^0 [45]. After introducing ceria into the silica the sample CeO_2/HMS shows distinct hydrogen uptake peaks, demonstrating the reducible nature of the support. The first peak at 50 °C should be due to the reduction of the surface oxygen on ceria [44]. Ying et al. [46] interpreted that the peak (from 350 to 600 °C) is due to the reduction of surface-capping oxygen of CeO_2, and the peak observed above 600 °C is typical of the reduction of bulk-phase lattice oxygen. Qusmane et al. [47] attributed the peak at 440 °C to the reduction of surface ceria not interacting with gold while reduction of bulk ceria occurs at 820 °C. So the peaks of 400 and 600 °C correspond to the reduction of surface-capping oxygen and surface ceria not interacting with gold.

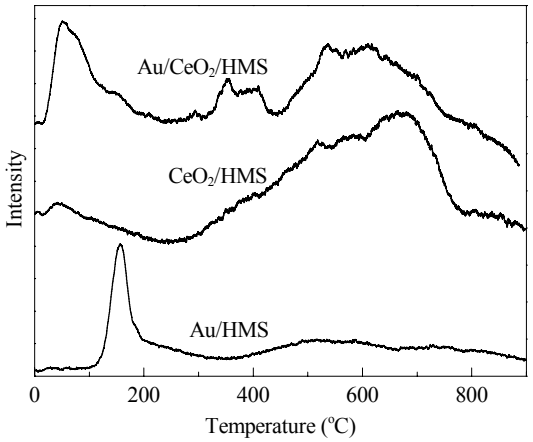

Fig. 8. H_2-TPR profiles of Au/HMS, CeO_2/HMS, and Au/CeO_2/HMS. Signal intensities of Au/HMS are reduced to 50% of the original intensities.

After gold loading, the reduction of Au^{3+} to Au^+/Au^0 and ceria in the Au/CeO_2/HMS catalyst is much easier. The lowering of the reduction temperature implies that the introduction of gold helps to weaken the surface oxygen bond in ceria, which means that the transfer of oxygen atoms across the solid-gas interface during the reaction is facilitated [8]. In addition, the presence of ceria on the silica has a strong impact on the formation and stability of supported metallic gold particles [45]. Above all, the composite catalyst works much like pure Au/CeO_2 [39].

Furthermore, DRIFT spectra of Au/CeO_2/HMS and Au/HMS were collected and the results are shown in Fig. 9. In Fig. 9(a) and (b) we can see the bands at 2800–3500 cm^{-1}, which can be ascribed to hydroxyl groups mainly on the ceria surface. Hydroxyl groups are proposed as the intermediate species during CO oxidation [49,50]. Generally, the presence of a band at 2112 cm^{-1} is assigned to CO ad-

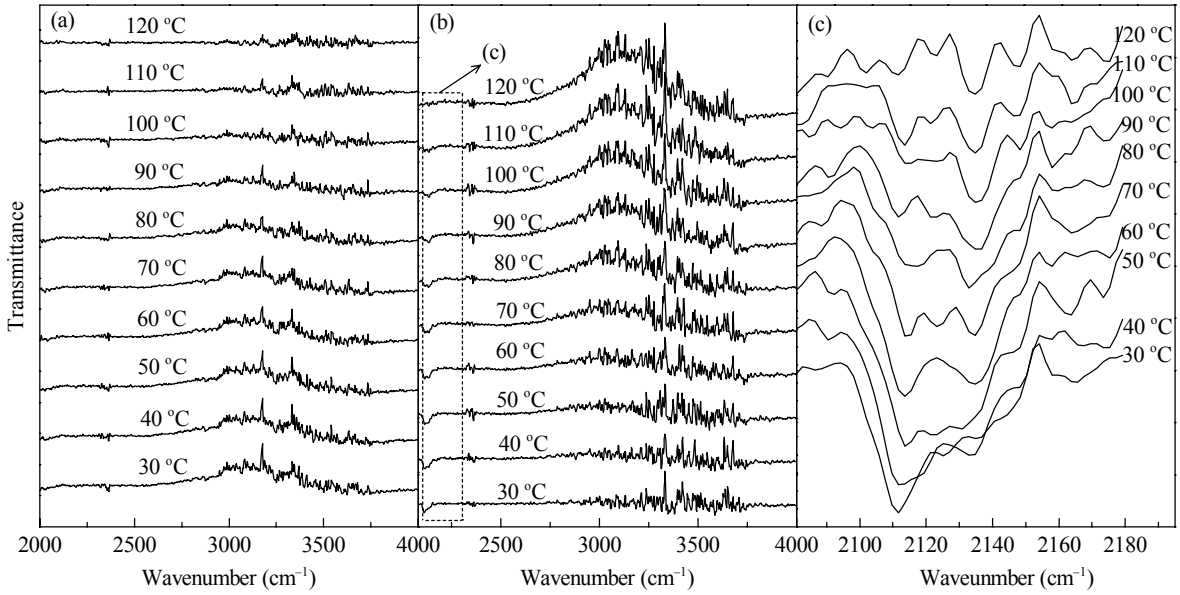

Fig. 9. DRIFT spectra of the Au/HMS (a) and Au/CeO_2/HMS (b, c) catalysts.

sorbed on metallic gold sites while a band of 2142 cm^{-1} indicates CO adsorbed on cationic gold [51]. However, the CO interacting with the CeO_2 support also yields a characteristic IR band at about 2133 cm^{-1} for Ce^{3+} ions [36,52] and 2148 cm^{-1} for Ce^{4+} ions [53], respectively. From Fig. 9(a) one can see that the sample Au/HMS does not show any bands of CO adsorbed on metallic or cationic gold sites within the temperature range of 30–120 °C. This is in agreement with the catalytic activity result of Au/HMS (Fig. 4). After introducing ceria into the silica the Au/CeO_2/HMS shows CO adsorption at bands of 2114 cm^{-1} (metallic gold) and 2136 cm^{-1} (cationic gold, Fig. 9(b)). The bands at 2136 cm^{-1} can also be related to CO adsorptions on Ce^{3+} ions of the CeO_2 support. Considering the Au/CeO_2/HMS was pretreated in a mixed atmosphere of nitrogen and hydrogen at 250 °C for 2 h before DRIFT measurement, the band at 2136 cm^{-1} should assigned to the CO adsorption on Ce^{3+} ions. After magnification of this part as Fig. 9(c) it can be seen that upon increasing the reaction temperature, the band at 2114 cm^{-1} becomes gradually weaker, demonstrating a lower steady state amount of CO being present on the catalyst, i.e. the adsorbed CO is more rapidly removed again by oxidation.

The chemical states of the Au species on fresh, reduced, and spent catalysts were investigated by XPS. The fitted Au 4*f* curve of the spectrum of the fresh catalyst (Fig. 10) consists of distinct peaks. The doublet at 83.6 and 87.4 eV is the feature of metallic Au^0 species [54]. The doublet at 85.6 and 89.2 eV is assigned to cationic $Au^{\delta+}$ species. The atomic ratio of $Au^{\delta+}$/Au of this catalyst is 0.54, which was calculated based on the peak areas of $Au^{\delta+}$ and metallic Au. The XPS profiles of Au/CeO_2/HMS after the reduction and catalytic test show a doublet at 83.0 and 86.8 eV with a BE shift of –0.6 eV, which can be assigned to metallic gold species. The negative BE shift of Au 4*f* indicates that the gold nanoparticles possess negative charges, which could be related to the interaction between gold nanoparticles and oxygen vacancies of ceria [55], as reflected in the H_2-TPR results.

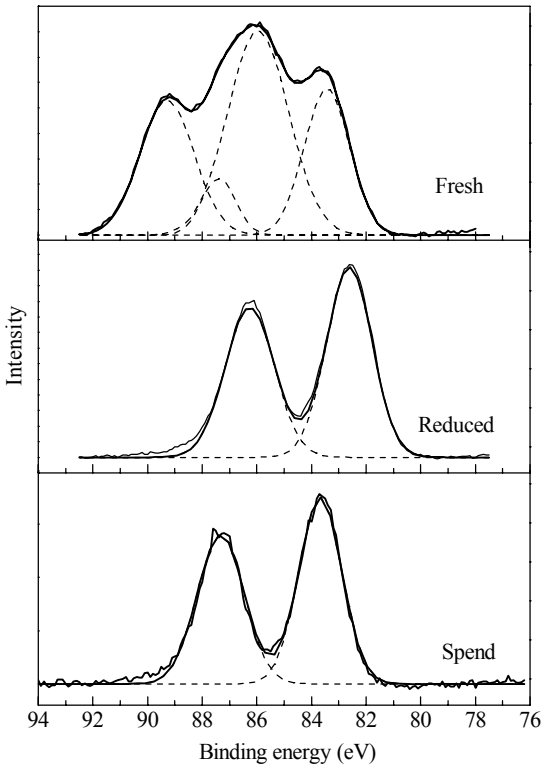

Fig. 10. XPS profiles of fresh, reduced, and used Au/CeO_2/HMS.

The nature of the active sites and oxidation state of the catalytically active Au species are still controversial in the literature. For example, Costello et al. [56] believe that Au^0 is necessary for catalytic activity in CO oxidation, while Guzman et al. [57] proposed that the cationic gold species are responsible for CO oxidation. Even when the same support was used, contradictory results concerning the role of the Au species in CO oxidation were obtained [49,58]. From the present investigation, combining the results of the XPS and in-situ DRIFT measurements, one can conclude that CO is only adsorbed and activated by metallic gold on the Au/CeO_2/HMS catalyst. A possible explanation could be that the highly dispersed metallic gold nanoparticles can activate CO and the small ceria nanoparticles supply oxygen in the reaction.

3 Conclusions

The hierarchically nanostructured composite Au/CeO_2/HMS was fabricated and exhibited a high CO oxidation activity. The presence of ceria had a significant effect on controlled on target deposition and the stabilization of small metallic gold nanoparticles on the silica support. The interaction between gold and ceria was verified by H_2-TPR, DRIFT, and XPS. It can be concluded that CO was only adsorbed and activated by metallic gold. The highly dispersed metallic gold nanoparticles can activate CO and the small ceria nanoparticles supply oxygen in the reaction. The presence of silica improved the stability of the gold catalyst.

Acknowledgement

We are highly grateful to Prof. F. Schüth for helpful discussion and to Mr. B. Spliethoff for TEM measurements.

References

1 Haruta M, Yamada N, Kobayashi T, Iijima S. *J Catal*, 1989, **115**: 301
2 Chen Z, Gao Q M. *Appl Catal B*, 2008, **84**: 790
3 Wang G H, Li W C, Jia K M, Spliethoff B, Schüth F, Lu A H. *Appl Catal A*, 2009, **364**: 42
4 Yoon B, Häkkinen H, Landman U, Wörz A S, Antonietti J M, Abbet S, Judai K, Heiz U. *Science*, 2005, **307**: 403
5 Hayashi T, Tanaka K, Haruta M. *J Catal*, 1998, **178**: 566
6 Bailie J E, Hutchings G J. *Chem Commun*, 1999: 2151
7 Tabakova T, Idakiev V, Andreeva D, Mitov I. *Appl Catal A*, 2000, **202**: 91
8 Yan L, Zhang X M, Ren T, Zhang H P, Wang X L, Suo J H. *Chem Commun*, 2002: 860
9 Costello C K, Kung M C, Oh H S, Wang Y, Kung H H. *Appl Catal A*, 2002, **232**: 159
10 Guo Q L, Luo K, Davis K A, Goodman D W. *Surf Interface Anal*, 2001, **32**: 161
11 Wang G Y, Lian H L, Zhang W X, Jiang D Z, Wu T H. *Kinet Catal*, 2002, **43**: 433
12 Kim C H, Thompson L T. *J Catal*, 2005, **230**: 66
13 Zhu H G, Ma Z, Clark J C, Pan Z W, Overbury S H, Dai S. *Appl Catal A*, 2007, **326**: 89
14 Wang H P, Liu C J. *Appl Catal B*, 2011, **106**: 672
15 Wolf A, Schüth F. *Appl Catal A*, 2002, **226**: 1
16 Penkova A, Martínez Blanes J M, Cruz S A, Centeno M A, Hadjiivanov K, Odriozola J A. *Microporous Mesoporous Mater*, 2009, **117**: 530
17 Lee B, Ma Z, Zhang Z T, Park C, Dai S. *Microporous Mesoporous Mater*, 2009, **122**: 160
18 Zhu H G, Liang C D, Yan W F, Overbury S H, Dai S. *J Phys Chem B*, 2006, **110**: 10842
19 Veith G M, Lupini A R, Rashkeev S, Pennycook S J, Mullins D R, Schwartz V, Bridges C A, Dudney N J. *J Catal*, 2009, **262**: 92
20 Okumura M, Nakamura S, Tsubota S, Nakamura T, Azuma M, Haruta M. *Catal Lett*, 1998, **51**: 53
21 Hu J C, Chen L F, Zhu K K, Suchopar A, Richards R. *Catal Today*, 2007, **122**: 277
22 Magureanu M, Mandache N B, Hu J C, Richards R, Florea M, Parvulescu V I. *Appl Catal B*, 2007, **76**: 275
23 Lu G M, Ji D, Qian G, Qi Y X, Wang X L, Suo J S. *Appl Catal A*, 2005, **280**: 175
24 Lee B, Zhu H, Zhang Z, Overbury S H, Dai S. *Microporous Mesoporous Mater*, 2004, **70**: 71
25 Zhu H, Lee B, Dai S, Overbury S H. *Langmuir*, 2003, **19**: 3974
26 Aprile C, Abad A, García H, Corma A. *J Mater Chem*, 2005, **15**: 4408
27 Kónya Z, Puntes V F, Kiricsi I, Zhu J, Ager III J W, Ko M K, Frei H, Alivisatos P, Somorjai G A. *Chem Mater*, 2003, **15**:1242
28 Zhu J, Kónya Z, Puntes V F, Kiricsi I, Miao C X, Ager J W, Alivisatos A P, Somorjai G A. *Langmuir*, 2003, **19**: 4396
29 Lin H P, Chi Y S, Lin J N, Mou C Y, Wan B Z. *Chem Lett*, 2001: 1116
30 苏继新, 张慎平, 马丽媛, 屈文, 张明博. 催化学报 (Su J X, Zhang Sh P, Ma L Y, Qu W, Zhang M B. *Chin J Catal*), 2010, **31**: 839
31 Qian K, Huang W X, Jiang Z Q, Sun H X. *J Catal*, 2007, **248**: 137
32 Qian K, Huang W X, Fang J, Lv S S, He B, Jiang Z Q, Wei S Q. *J Catal*, 2008, **255**: 269
33 Qian K, Zhang W H, Sun H X, Fang J, He B, Ma Y S, Jiang Z Q, Wei S Q, Yang J L, Huang W X. *J Catal*, 2011, **277**: 95
34 Zou X H, Xu J G, Qi S X, Suo Z H, An L D, Li F. *J Nat Gas Chem*, 2011, **20**: 41
35 单文娟, 刘畅, 郭红娟, 杨利华, 王晓楠, 冯兆池. 催化学报 (Shan W J, Liu Ch, Guo H J, Yang L H, Wang X N, Feng

Zh Ch. *Chin J Catal*), 2011, **32**: 1336
36 Carrettin S, Concepción P, Corma A, López Nieto J M, Puntes V F. *Angew Chem*, *Int Ed*, 2004, **43**: 2538
37 Moreau F, Bond G C, Vander Linden B, Silberova B A A, Makkee M. *Appl Catal A*, 2008, **347**: 208
38 Qian K, Lva S S, Xiao X Y, Sun H X, Lu J Q, Luo M F, Huang W X. *J Mol Catal A*, 2009, **306**: 40
39 Smått J H, Schunk S, Lindén M. *Chem Mater*, 2003, **15**: 2354
40 Lu A H, Smått J H, Lindén M. *Adv Funct Mater*, 2005, **15**: 865
41 Somodi F, Borbáth I, Hegedús M, Tompos A, Sajó I E, Szegedi A, Rojas S, Fierro J L G, Margitfalvi J L. *Appl Catal A*, 2008, **347**: 216
42 Zhang R R, Ren L H, Lu A H, Li W C. *Catal Commun*, 2011, **13**: 18
43 Haruta M. *Gold Bull*, 2004, **37**: 27
44 Pillai U R, Deevi S. *Appl Catal A*, 2006, **299**: 266
45 Hernandez J A, Pawelec S G B, Zepeda T A. *Appl Catal B*, 2009, **89**: 128
46 Ying F, Wang S J, Au C T, Lai S Y. *Microporous Mesoporous Mater*, 2011, **142**: 308
47 Ousmane M, Liotta L F, Di Carlo G, Pantaleo G, Venezia A M, Deganello G, Retailleau L, Boreave A, Giroir-Fendler A. *Appl Catal B*, 2011, **101**: 629
48 Fu Q, Kudriavtseva S, Saltsburg H, Flytzani-Stephanopoulos M. *Chem Eng J*, 2003, **93**: 41
49 Romero-Sarria F, Martínez T L M, Centeno M A, Odriozola J A. *J Phys Chem C*, 2007, **111**: 14469
50 Karpenko A, Denkwitz Y, Plzak V, Cai J, Leppelt R, Schumacher B, Behm R J. *Catal Lett*, 2007, **116**: 105
51 Wu Z L, Zhou S H, Zhu H G, Dai S, Overbury S H. *J Phys Chem C*, 2009, **113**: 3726
52 Tabakova T, Boccuzzi F, Manzoli M, Andreeva D. *Appl Catal A*, 2006, **252**: 385
53 Concepción P, Carrettin S, Corma A. *Appl Catal A*, 2006, **307**: 42
54 Park E D, Lee J S. *J Catal*, 1999, **186**: 1
55 Vindigni F, Manzoli M, Chiorino A, Boccuzzi F. *Gold Bull*, 2009, **42**: 106
56 Costello C K, Guzman J, Yang J H, Wang Y M, Kung M C, Gates B C, Kung H H. *J Phys Chem B*, 2004, **108**: 12529
57 Guzman J, Gates B C. *J Am Chem Soc*, 2004, **126**: 2672
58 Dekkers M A P, Lippits M J, Nieuwenhuys B E. *Catal Lett*, 1998, **56**: 195